AIAA-2003-0493

Modeling the Effect of Plasma-Wall Interaction in a Hall Thruster

Subrata Roy* and B. P. Pandey**
Computational Plasma Dynamics Laboratory
Kettering University, Flint, MI

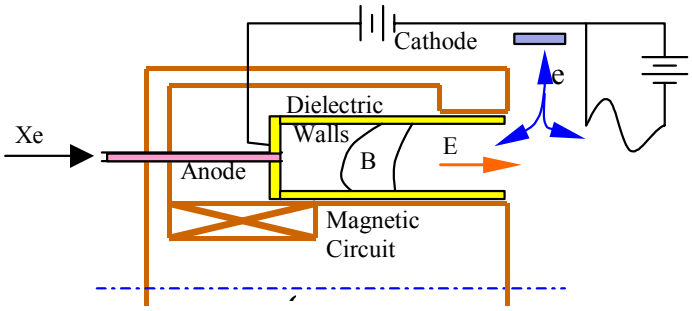

41st Aerospace Sciences Meeting and Exhibit
6-9 January 2003
Reno, Nevada

Modeling the Effect of Plasma-Wall Interaction in a Hall Thruster

Subrata Roy* **and B. P. Pandey§**

Computational Plasma Dynamics Research Laboratory
Kettering University, Flint, MI 48504

Among many reasons limiting the efficiency and lifetime of a Hall thruster, the most critical is the wear of the surface layer of the ceramic walls due to the plasma-wall interactions. The plasma-wall interaction is a function of wall potential, which in turn is determined by the secondary electron emission and sputtering yield. In this paper, we document the numerical result of the Hall thruster dynamics in the presence of plasma-wall interaction in one and two-dimensional framework. A comparison is made with the two dimensional simulation. The changes in the plasma density, the potential and the azimuthal electron velocity due to the sputter yield are significant in the acceleration region. The plasma number density, temperature, velocity and potential decrease in the presence of the SEE and the sputter yield. However, the neutral number density and the velocity do not exhibit any significant change. The neutral velocity, which decreases initially, starts increasing toward the exit consistent with the computed neutral density profile. Numerical potential distribution shows a good agreement with experimental data reported in the literature.

INTRODUCTION

The stationary plasma thruster (SPT) is a type of Hall thruster that belongs to a class of propulsion devices collectively referred to as the electric propulsion devices. The energy used in the propulsion in such a device is derived from the electrostatic energy of the plasma. A schematic of the SPT, shown in Fig. 1 describes an annular geometry with a rear end anode and an external hollow cathode. Concentric dielectric walls bound the acceleration channel. Hall thrusters rely on the large potential fields to accelerate the ionized gas. By applying a voltage between the anode and the cathode, an external axial electric field is imposed. As the electrons move upstream towards the anode from the cathode, their motion is impeded by the strong radial magnetic field.

Because of the axial electric and the radial magnetic fields, the electrons drift forming an azimuthal Hall current. These electrons are also responsible for ionizing the propellant atoms that are injected through the anode and subsequently accelerated by the axial electric field. The magnetic field suppresses the axial mobility of the electrons causing high impedance in the axial direction. This axial impedance helps maintain an electric field between the anode and the cathode. Ions on the other hand have a larger gyration radius than the SPT scale and therefore, will behave as

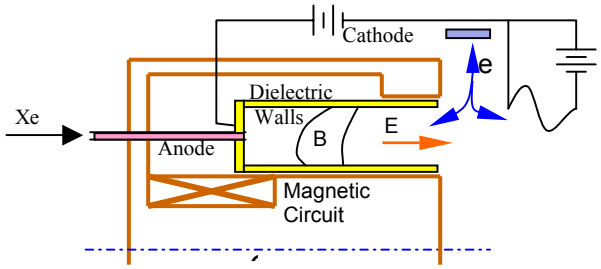

Figure 1. Hall thruster schematic.

if there is no radial magnetic field. This will result in the ions streaming out of the device, accelerating down the potential like unmagnetized plasma. Electrons from the external cathode neutralize this emerging ion flux.

* Assistant Professor, Department of Mechanical Engineering, E-mail: sroy@kettering.edu, Associate Fellow, AIAA
§ Post-doctoral Research Fellow, E-mail: bpandey@kettering.edu, Member, AIAA

The reason for the Hall thruster's popularity lies in its performance and efficiency. It has superior thrust than other types of stationary thrusters since its acceleration is not inhibited by the space charge field in the quasi-neutral plasma.[1,2] Present day Hall thrusters offer specific impulses ranging 1600 s to 2000 s with 80 mN to ~1N thrust for power exceeding 4.0 kW. The efficiency of a typical optimized Hall thruster is about 50% or more and can operate over a wide range of currents. Increasing the efficiency of the Hall thruster while having a lifetime of close to 8000 hrs is a challenge, as the choice of the thruster size requires an optimum selection between the efficiency and the lifetime.[3,4] The near wall plasma processes remain to be investigated in detail to understand the lifetime limiting issues. For example, wall erosion of the thruster occurs due to the plasma-wall interactions. This may affect the plasma current, azimuthal momentum and internal energy. Further, the sputter yield from the wall may contaminate the spacecraft surface. The surface roughness of the wall plays an important role in the surface evolution under erosion. The secondary electron emission too can have significant effect on the SPT performance. The "intermediate" energy electrons are responsible for the ejection of secondaries from the wall.[1] The secondary emission could lead to the charge saturation of the sheath[5] and may be responsible for the sheath instability.[1]

Numerical simulation of the plasma dynamics of a Hall thruster is an invaluable tool as it can mimic the real flight condition and has been carried out recently by several authors in the framework of the hybrid as well as the fluid models.[6-16] A two-dimensional (2D) finite element formulation of completely ionized plasma has been given recently.[14] The one-dimensional (1D) model of partially ionized plasma incorporating the neutral dynamics and the effect of inelastic processes has also been documented.[15,16] Present study generalizes the 1D finite element model[16] where the effect of sputtering yield and secondary emission on the dynamics was investigated in the presence of positive wall potential. However, very often, the potential at the dielectric wall is negative and therefore, 1D model of Roy and Pandey[16] needs to be generalized. Further, unlike our previous work,[16] this paper presents the isolated effect of the secondary electron emission and the sputtering yield on the plasma dynamics before investigating the combined effect of both. It is hoped that these results will provide basic understanding of the underlying physics of the acceleration channel inside the Hall thruster. In section II, we discuss the basic model of the thruster plasma. In section III, basic equations are given. The numerical results are documented in section IV. Finally, section V contains conclusion and future work recommendations.

PHYSICAL MODEL

The Hall thruster plasma is partially ionized gas, consisting of electrons, ions and neutral particles. In such a partially ionized plasma, several important elastic and inelastic processes can take place simultaneously. The elastic collision involves only exchange of momentum and energy between colliding particles whereas inelastic process e.g. ionization, recombination, charge-exchange collision, secondary emission, sputtering etc. can be responsible for redistributing the number density, momentum and energy of the particles. As described in appendix, not all processes are equally probable. For example, momentum exchange between electron-electron and ion-ion will not be important in comparison with the electron-ion momentum exchange as the relative drift between similar particles is small in comparison with the drift between electrons and ions.

The neutral gas used in the Hall thruster is typically Xenon, which is supplied externally through the inlet/anode. Near the anode, plasma is formed through collisional ionization via electron impact to the incoming neutral propellant. The plasma is assumed quasi-neutral, i.e. locally the electron number density n_e is equal to the ion number density n_i, as the Debye length is considerably smaller than the width of the thruster channel. The assumption of quasi-neutrality is valid except near the thin sheath layer. In the present work, sheath dynamics will not be taken into consideration and thus, plasma will be assumed quasi-neutral in the whole computational domain.

THEORETICAL FORMULATION

We shall assume that the ions are unmagnetized, since for typical parameters of a thruster plasma viz., magnetic field B ~ 200G and ion velocity 4×10^3 m/s the gyration radius of ions are about 0.1 m, which is much larger than the size of the thruster (0.02 – 0.03 m). Therefore, the effect of magnetic field on the ion transport will be ignored.

The pressure term in the ion momentum equation can be ignored as the thermal energy of the ions is much smaller than their kinetic energy i.e. $T_i << m_i V_i^2$. Note that owing to the small inertia, electron response time is much faster than the ion response time. As a result, electrons will attain the steady state faster than the ions. Keeping this in mind, electron momentum and energy equations are solved at steady state, whereas for ions and neutrals, a set of time independent continuity and momentum equations are simultaneously solved. The axisymmetric cylindrical thruster plasma is modeled by the 1D geometry where z corresponds to the axial direction and θ is along the azimuth. The variation in the radial direction is assumed negligible as compared to axial changes. Following one-dimensional equations are solved in the present work.

Electron momentum equation:

$$V_{ez}\frac{\partial V_{ez}}{\partial z} = -\frac{1}{m_e n_e}\frac{\partial}{\partial z}(p_e) - \frac{e}{m_e}E_z - \left(\frac{\omega_c^2}{\nu_{ei}+\nu_{en}+\alpha_B\omega_c}\right)V_{ez} \quad (1)$$
$$-\nu_{ei}(V_{ez}-V_{iz}) - \nu_{en}(V_{ez}-V_{nz}) - \left(\frac{S}{n_e}\right)(V_{ez}-V_{nz}) + \nu_w V_{ez}.$$

where m_e is the electron mass, n_e is the electron number density. V_{ez}, V_{iz}, V_{nz} are respective electron, ion and neutral axial velocities. $V_\theta = E_z/B_r$ is the azimuthal electron drift velocity, E_z is the axial electric field and B_r radial magnetic field, $p_e = n_e T_e$ is the electron pressure with T_e as the electron temperature in eV, $\omega_c = eB_r/m_e$ is the electron-cyclotron frequency, and the source term due to the ionization, recombination and the charge exchange is $S = S_{recomb} + S_{ioniz} + S_{cex.}$ Following relation between azimuthal and axial velocities is utilized,

$$V_{e\theta} = \left(\frac{\omega_c}{\nu_{ei}+\nu_{en}+\alpha_B\omega_c}\right)V_{ez} = \Omega V_{ez}. \quad (2)$$

where, α_B is the Bohm diffusion coefficient and Ω is the Hall parameter. It is known that the classical short-range, binary collision between plasma particles ν_{ei} and plasma-neutrals ν_{en} are not sufficient to explain the plasma behavior observed in the thruster and either by invoking Bohm diffusion[8] or by invoking plasma-wall interaction,[1,8] such a behavior is explained. We model plasma wall interaction by introducing the electron-wall collision frequency ν_w. Further, the effect of anomalous Bohm conductivity has been included qualitatively by including the equivalent frequency $\nu_B = \alpha_B \omega_c$, that incorporates the effect of magnetic field fluctuations. The Bohm parameter α_B is related to the anomalous diffusion of the electron across the magnetic field. Different authors[8,11,13] have used different values of α_B ranging between 16 to 100. In the present work we shall assume $\alpha_B = 16$. Typical value of Hall parameter varies between 100 – 1000. The electron-wall frequency has been modeled by the last term in the equation (1), where ν_w for a channel of width h is given as

$$\nu_w = \begin{cases} \dfrac{2V_{the}}{h}e^{\varphi'}\left(\dfrac{1-\delta}{1-Y}\right); & \varphi' \le 0, \\ \dfrac{2V_{the}}{h} & ;\varphi' \ge 0. \end{cases} \quad (3)$$

Here $\varphi' \equiv -|e|\varphi'/T_e$ is the normalized wall potential, $V_{the} = (T_e/2\,\pi\,m_e)^{1/2}$ is the electron thermal velocity, and, δ and Y are coefficients of the secondary emission and the ion sputter yield respectively. The expression for the near wall sheath potential is found by balancing the ion flux ($\Gamma_i = n_i V_i$) with the electron flux ($\Gamma_e = n_e V_e$), i.e. $\Gamma_i(1-Y) = \Gamma_e(1-\delta)$. Then, the normalized wall potential is given as,

$$\varphi' = -\left[0.5 + \ln\left\{\frac{(1-\delta)}{(1-Y)}\left(\frac{m_i}{2\pi m_e}\right)^{1/2}\right\}\right] \quad (4)$$

Based on the experimental observations, we shall use an empirical formula used for sputter yield,[17]

$$Y = \frac{S}{H_s}(T_i - 4H_s), \quad (5)$$

where $S = 1\times10^{-2}$ is the sputtering yield factor,[18] H_s = 3000 K is the sublimation energy of boron nitride and T_i is the incident ion energy on the target. In the present work, we shall assume $T_i = 0.1\ T_e$. The secondary electron emission coefficient for Boron nitride wall is given as,[10]

$$\delta = \left(\frac{T_e}{E_w}\right)^p. \quad (6)$$

Here E_w = 16.64 eV for p = 0.576 and E_w = 17.0 eV for p = 0.5.

The dynamics of the electron is determined by the pressure gradient, by the electric and magnetic forces and by the collisional exchange of momentum in equation (1). The convective term in equation (1) retains the effect of the electron inertia. The contribution of the electron inertia is small and on this ground, its effect on the plasma dynamics is generally ignored.[8] However, in the regions of sharp flow gradients, the effect of convective term may become

finite and therefore, the convective term is retained in this formulation. Similarly, since collision time scales are much slower than the electron-cyclotron gyration time scale, one may ignore elastic and inelastic collision terms in comparison with the Lorentz force term $V_z \times B_r$ in the momentum equation. Such an approach, will exclude the dynamics of the momentum exchange as well as the effect of ionization and recombination, severely limiting the applicability of the model to the thruster plasma. Therefore, all the collision terms are retained in the electron momentum equation (1).

Neglecting the effect of radiation, viscous dissipation and thermal conduction, electron energy equation can be written as

$$\frac{d}{dz}\left[n_e V_{ez}\left\{\frac{m_e(1+\Omega^2)V_{ez}^2}{2}+\frac{5}{2}T_e\right\}\right]-n_e e V_{ez}\frac{d\varphi}{dz}$$
$$=3\frac{m_e}{m_i}n_e\nu_{ei}(T_i-T_e)+3\frac{m_e}{m_n}n_e\nu_{en}(T_n-T_e)+S\left(\frac{3}{2}T_e+\alpha E_I\right) \quad (7)$$
$$-n_e\nu_w E'$$

Here T_e , T_i and T_n (~.3 eV) are electron, ion and neutral temperatures in eV, respectively, and E_I is the ionization energy of the Xenon.

Equation (7) includes the effect of the Joule heating, contribution due to the exchange of random thermal energy and due to the ionization and recombination and interaction of the plasma with the wall. The convective flux of the kinetic energy includes the flux of the azimuthal electron kinetic energy $V^2 = V_{ez}^2 + V_{e\theta}^2 = (1+\Omega^2)V_{ez}^2$. The value of α is between (2 –3) (Ref. 8) and

$$\nu_w E' = \begin{cases} \frac{2T_e V_{the}}{h}e^{\varphi'}\left[\left(2-\varphi'\right)-\delta\left(2\frac{T_{se}}{T_e}-\varphi'\right)\right]; & \varphi' \le 0, \\ \frac{4T_e V_{the}}{h}\left(1-2\frac{T_{se}}{T_e}\right); & \varphi' \ge 0. \end{cases} \quad (8)$$

Here, T_{se} is the temperature of secondary electrons and assumed to be of the order of 0.1 T_e.

Ion continuity:

$$\frac{\partial n_i}{\partial t}+\frac{\partial(n_i V_{iz})}{\partial z}=S-\nu_w n_i \quad , \quad (9)$$

ion momentum:

$$\frac{\partial V_{iz}}{\partial t}+V_{iz}\frac{\partial V_{iz}}{\partial z}=\left(\frac{e}{m_i}\right)E_z+\left(\frac{m_e}{m_i}\right)\nu_{ei}(V_{ez}-V_{iz}) \quad (10)$$
$$-\left(\frac{m_n}{m_i}\right)\nu_{in}(V_{iz}-V_{nz})-\left(\frac{S}{n_e}\right)V_{iz}+\nu_w V_{iz}$$

and neutral continuity:

$$\frac{\partial n_n}{\partial t}+\frac{\partial(n_n V_{nz})}{\partial z}=-S_n. \quad (11)$$

Here, $S_n = S_{recomb} + S_{n,ioniz} + S_{cex}$ and $S_{n,ioniz} = k_i^{0+} n_e n_n + k_i^{0++} n_e n_n$. Equations (1)-(11) are supplemented with the current and mass conservation equations respectively as,

$$en_i(V_i - V_e) = J_T, \quad (12)$$

$$m_n n_n V_{nz} + m_i n_i V_{iz} = \frac{\dot{m}}{A}. \quad (13)$$

Here $J_T = I_d/A$ is the total current density; I_d is the total discharge current, A is the cross section of the thruster channel and $\dot{m}$ is the mass flow rate.

Before numerically solving above set of basic equations (1)-(13), the physical variables are normalized using experimental data. The mass flow rate of the propellant is $\dot{m} = \rho V A$. The flux of the propellant is $\Gamma = 10^{23}$ m^{-2} s^{-1}. Temperature T_e is normalized to the first ionization potential of Xenon, $T_* = E_I = 12.1$ eV. Then all dependent variables can be normalized by using their reference values, $V_* = \sqrt{(T_*/m_i)} = 4\times10^3$ m/s, $n_* = \Gamma/V_* = 2.5\times10^{19}$ m^{-3}, and $\nu_* = \sigma_* \Gamma_*$ s^{-1} where $\sigma_* = \sigma_0\sqrt{(m_i/m_e)}$, $\sigma_0 \cong 3.6\times10^{-20}$ m^2 for Xe. The fundamental length scale can be defined in terms of the characteristic velocity and collisional frequency as, $l_0 = V_*/\nu_*$. The time scale is $t_0 = \nu_*^{-1}$.

BOUNDARY CONDITIONS

Since the results of the simulation are highly sensitive to the initial and boundary conditions on the plasma density, velocity, potential and electron temperature, proper initial and boundary conditions are adopted. Here the 1D radial magnetic field geometry is considered. In a typical Hall thruster experiment, radial field is dominant in comparison with the axial field. A shifted Gaussian (bell shaped) magnetic field profile is assumed, which reaches maximum at the exit plane

$$B_r(z) = B_0(z) + B_{\max}\exp(-(z-z_{exit})^2) \quad (14).$$

The magnetic field profile is given in Fig. 2. It is clear from the figure that magnetic field has a maximum near the exit plane.

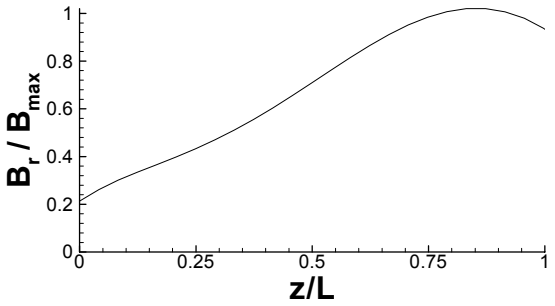

Figure 2. Imposed magnetic field distribution.

At the inlet, the neutral number density is assumed equal to the reference density n_* and the plasma density is fixed $n_i = 0.14 n_*$. The axial ion velocity is not fixed at the inlet. Under typical conditions, next to anode, a plasma sheath (typical width ~ Debye length) forms and ions must flow into the sheath from the quasi-neutral region. The axial velocity is near zero close to the anode and then begins to rise at the edge of the acceleration zone and reaches maximum velocity beyond the exit.[19] Such flow behavior has also been observed in the classical nozzle problem, where flow changes smoothly from subsonic (in the narrow region) to supersonic in the divergent region. Therefore, at the exit the flow velocity should at least attain the characteristic speed of the medium, i.e., the sonic point. In conformity with the available experimental results and the numerical model[8], we impose ion velocity at the exit boundary, whereas electron velocity is assumed zero at the inlet. At the inlet, a homogeneous Neumann condition for electrostatic potential is imposed. At the downstream boundary (thruster exit plane), we specify an electron temperature T_e = 10 eV, that is close to the experimental results.[19,20] Since at the cathode, potential is zero, a vanishing potential is assumed at the outlet. For neutral and ion densities along with the electron velocity, a homogeneous Neumann condition is assumed at the exit. The velocity of the neutral is consistently calculated from the mass flow equation.

In the present work, a 1D finite element formulation is used to solve equations (1)-(13). Solutions to corresponding 2D extension of the problem are also reported. The detailed description of the numerical algorithm is given elsewhere.[15,16,22] The choice of time step is dictated by the Courant-Fredrich-Levy condition.[23] The code uses variable time steps till the transient features die down as the iteration converges to a steady state. The solution is declared convergent when the maximum residual for each of the state variable becomes smaller than a chosen convergence criterion of $\in=10^{-4}$. Here, the convergence of a solution vector **U** on node *j* is defined as the norm:

$$\frac{\|\mathbf{U}_j - \mathbf{U}_{j-1}\|}{\|\mathbf{U}_j\|} \leq \in \qquad (15)$$

RESULTS AND DISCUSSION

Equation set (1)-(13) has been solved over a computational domain (z/L:0,1) where L is the channel length with the exit plane located at 2 cm. The mesh consists of 40 equal length 1-D quadratic finite elements (i.e., 81 nodes) for all numerical results presented here.

The plasma density profiles are given in Fig. 3a, 3b and 4. In Fig. 3a, plasma number density is plotted for the values of SEE, δ = 0., 0.80, 0.90 and 0.95 in the absence of sputter yield, Y = 0. The number density (Fig. 3a) increases rapidly from 2.5×10^{17} to 10^{18} m^{-3} near the exit plane. We see that the plasma number density remains almost unaffected for δ = 0., 0.80. However, the effect of SEE becomes pronounced as δ increases, i.e., for δ = 0.90, 0.95. Similar effects of SEE on the plasma number density have been reported in the literature.[13] The decrease in the number density is consistent with the increase in δ. This is due to the fact that an increase in δ implies an increase in the plasma-wall interaction and hence, the loss of plasma particles. However, the relation between SEE and plasma number density is not a linear one. The increase in the SEE causes the decrease in the plasma temperature since most of the "intermediate-energy" primary electrons will be lost to the wall. This in turn will affect the ionization. As a result, plasma number density will decrease. Subsequently this will lead in the decrease of the secondary electron population itself.

In Fig. 3b, plasma number density is plotted in the absence of the SEE (δ = 0) and, for different values of Y. The effect of Y on plasma density is very pronounced, especially between Y = 0.6 and Y = 0.7. The decline in plasma density is dramatic for Y = 0.7. Recalling that the plasma wall interaction frequency varies as 1/(1 – Y), rapid decline in the number density appears as a result of the plasma-wall frequency becoming very large as Y crosses some critical value. In the present case, such a value is Y = 0.7.

In Fig. 4, plasma number density is plotted for various values of δ and Y. Curve (a) corresponds to δ = 0.8

and Y= 0; curve (b) corresponds to $\delta = \delta(T_e)$ and Y = 0.5; and curve (c) plots for $\delta = \delta(T_e)$ and Y= $Y(T_e)$. Interestingly, when both the SEE and the sputter yield are calculated self-consistently (curve c), plasma density is slightly higher than when only SEE is fixed and Y = 0 (curve a) or when both SEE and Y are fixed (curve b). Such a behavior indicates that the reduction in the plasma number density due to the temperature dependant calculation of Y and δ is less severe than when Y is switched off with δ fixed at a high value and when Y is 50% (curve a).

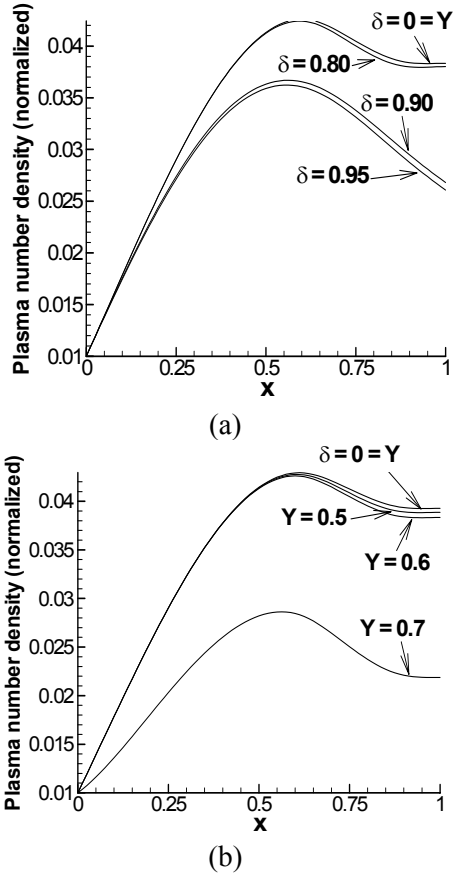

Figure 3. Normalized plasma density for the different values of secondary electron emission (SEE, δ) and sputter yield Y.

Such a behavior indicates that the sputter yield and secondary electron emission are intimately linked and they affect each other. The increase in the SEE leads to the decrease in the plasma density that in turn leads to the decrease in plasma temperature. The decreased plasma density will have lesser number of energetic ions and hence, a decrease in the sputter yield. The decreased plasma density will reduce the SEE. Therefore, the process of SEE, sputter yield and the process of ionization, recombination will regulate each other before the system reaches the steady state.

The rapid increase in the ion number density is reflected in the rapid decrease in the neutral number density (Fig. 5) from 2.5×10^{19} m^{-3} to approximately 2×10^{18} m^{-3}. This is consistent with the fact that as the neutral enters the thruster chamber it undergoes the impact ionization. The SEE (Fig. 5) and sputter yield Y (not shown) have almost no effect on the neutral density distribution except slightly near the exit. This result is expected, as there is no direct mechanism that could couple the plasma-wall interaction with the neutral dynamics of a SPT. The change in the neutral density does not exhibit the significant increase downstream of the channel as reported in other work.[13]

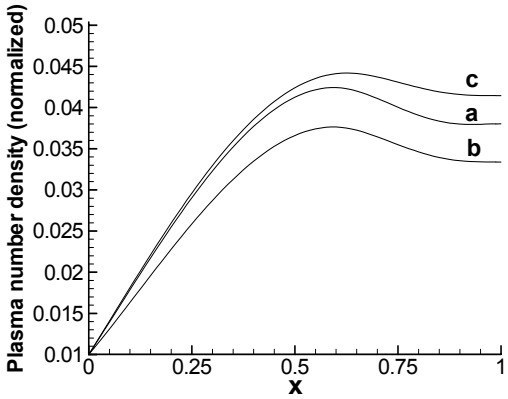

Figure 4. Normalized plasma density for various values of SEE and sputter yield. Curve (a) correspond to δ = 0.8 and Y = 0, curve (b) δ = Y = 0.5 and, curve (c) when SEE and Y, both are calculated self-consistently from the dynamics.

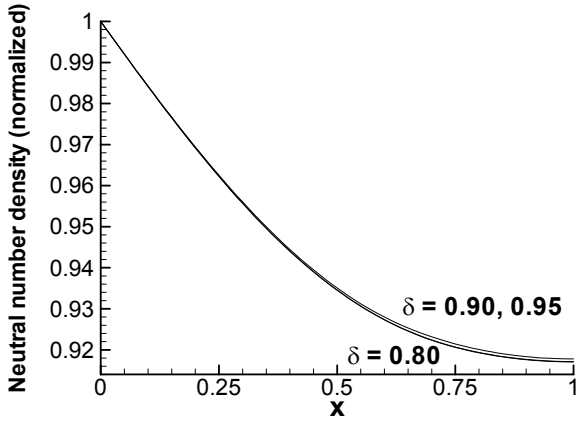

Figure 5. Neutral density in the presence of δ.

Fig. 6a describes the electron temperature profile for different values of SEE. The increase in the electron temperature is not uniform and the maximum increase

occurs just downstream of the center of the channel. The peak in the electron temperature can be attributed to the Ohmic heating due to the maximum gyration energy in this region. In the presence of temperature dependent SEE and sputter yield, the electron temperature is slightly lower than when $\delta = 0.80$, $Y = 0$. This result seems to suggest that due to the loss of "intermediate-energy" electrons (which are thought to be responsible for the SEE[1]), for $\delta = 0.80$, plasma is left with the fast electrons and thus, there is an increase in the electron temperature. Similar argument should hold for all values of δ. However, the number of "intermediate" electron reduces drastically for $\delta = 0.9$, 0.95 (Fig. 3a) and thus, despite the fast electrons being present in the channel, the mean temperature will decrease as seen in Fig. 6a. The 1D temperature profile computed using temperature dependent δ and Y is in agreement with the measured electron temperature near the exit.[19,20] Note that the experimental data reported in[19] has about 8% uncertainty. A better validation is expected in future 2D calculations.

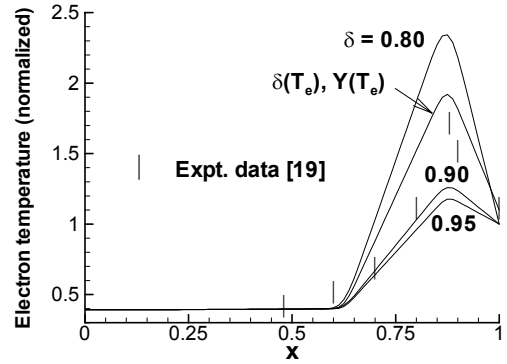

Figure 6. Effect of δ and Y on electron temperature.

In Fig. 6b, we plot electron temperature in the absence of secondary electron emission with different values of Y. The increase in Y is accompanied with the proportionate decrease in the electron temperature. This is consistent as the formula for the sputter yield (equation (5)) which uses a linear relationship between Y and electron temperature. The general profile of the temperature remains similar to the previous case.

Fig. 7 describes the ion and neutral velocity profiles for (a) $\delta = \delta(T_e)$, $Y = Y(T_e)$, (b) $\delta = 0.8$, $Y = Y(T_e)$, and (c) $\delta = 0.95$, $Y = 0$. When both SEE and sputter yield are calculated dynamically, we see that ion velocity generally is larger (curve a) than when, SEE is fixed and Y is calculated dynamically (curve b) or when SEE is fixed and there is no sputter yield (curve c). The increase in velocity for curve (a) is indicative of the fact that most of the intermediate energy ions and electrons are lost to the wall due to plasma-wall interaction and recombination. As a result, only highly accelerated particle will be left downstream of the channel. This inference is consistent with the neutral velocity profile (curve a), where, there is a slight increase in the velocity downstream of the channel. However, when SEE is fixed and Y is calculated dynamically (curve b), the velocity in the channel is lower than for curve (a). Similar behavior is also seen for fixed SEE in the absence of Y. Clearly, here the loss of "intermediate" energy particle is small, due to the smallness of Y and therefore, the ion velocity appears suppressed in comparison with curve (a). This interpretation is consistent with the neutral velocity profiles.

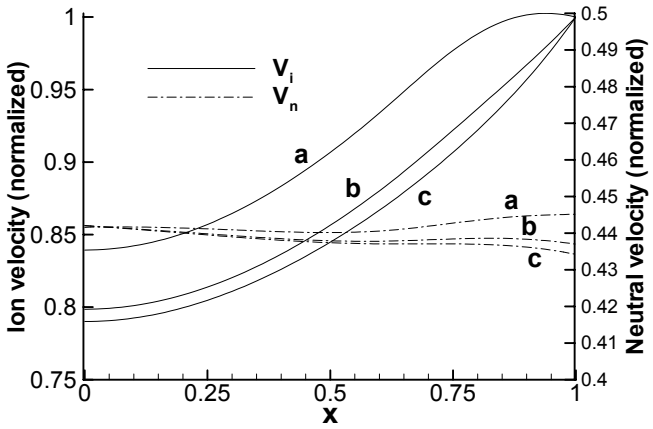

Figure 7. Ion and neutral velocities are given for (a) $\delta = \delta(T_e)$, $Y = Y(T_e)$, (b) $\delta = 0.8$, $Y = Y(T_e)$, and (c) $\delta = 0.95$, $Y = 0$.

In Figure 8, we plot the channel plasma potential $\phi - \phi_E$ when $\delta = \delta(T_e)$, $Y = Y(T_e)$. Here, ϕ_E denotes exit potential and is set equal to zero at cathode. The potential profile is similar to the case when $\delta = 0 = Y$. However, the value of potential decreases in the

presence of SEE and sputter yield. This is consistent since in the presence of SEE and Y, the plasma density gets affected. This in turn effects the current and hence the electric field in the plasma. Therefore, SEE and sputter yield reduces the plasma potential. Comparing with experimental data[19] for 200 V, which has an inaccuracy of ± 3 V, we see that the potential profile agrees very well with the observed data, especially inside the channel. Near the exit plane, the departure is not severe and we attribute the slight disagreement to the imposed zero exit ($\phi_E = 0$) boundary condition.

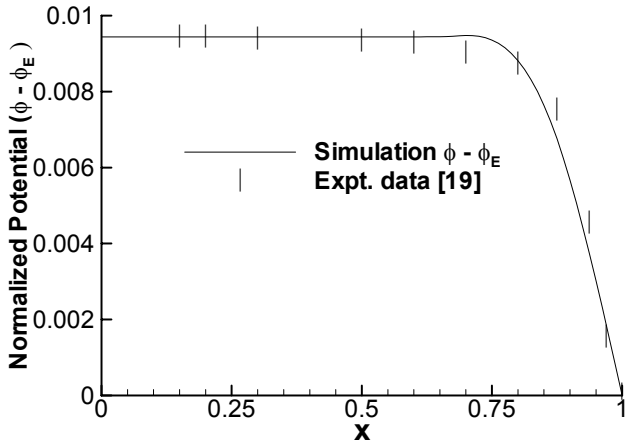

Figure 8. The plasma potential profile is given in the presence of SEE and sputter yield. The potential profile compares favorably with the experiment.[19]

In Figure 9, we plot SEE and sputter yield. We see that since δ (T_e) and $Y(T_e)$ are direct functions of the electron temperature, the curves have peak in the region where electron temperature is maximum. Further, the sputter yield is much smaller than the SEE. Therefore, the effect of SEE is more pronounced on the dynamics than sputter yield. However, for a few thousand hours thruster operation, sputtering will cause the significant erosion of the wall material and the yield Y will increase.

Present numerical model can be extended the 2D, 2D, three-fluid, partially ionized plasma model. Representative two-dimensional contours for plasma and neutral number densities for $\delta(T_e)$ and $Y(T_e)$ are plotted in Figures 10 and 11, respectively. The experimental results[20,21] show that the plasma density reaches its peak value inside the acceleration channel, near the inner wall before the exit plane. In this region, the radial magnetic field is the maximum and thus a large number of electrons are inhibited from moving in the axial direction, resulting in a high probability of impact ionization and plasma production. The maximum plasma density inside the acceleration channel agrees with the fact that the ionization channel is well inside the thruster. We note that virtually no breathing mode is observed between the peak of the plasma density and that of the electron temperature.

The neutral number density continues to decrease downstream up to the exit plane. Corresponding ion velocity distribution as shown in Figure 12 varies between 9 to 12 km/s.

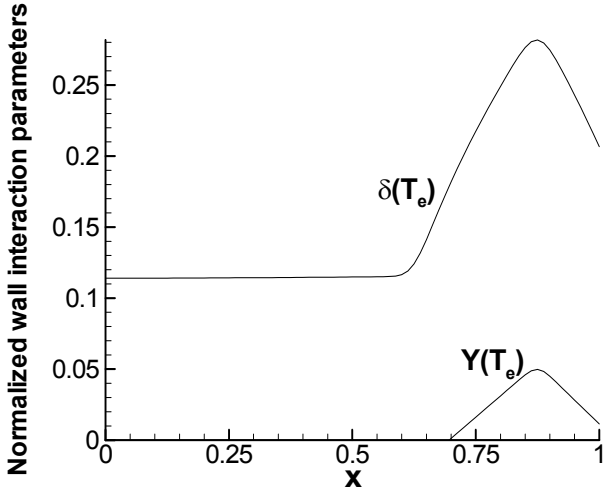

Figure 9. Profiles of SEE δ and sputter yield Y.

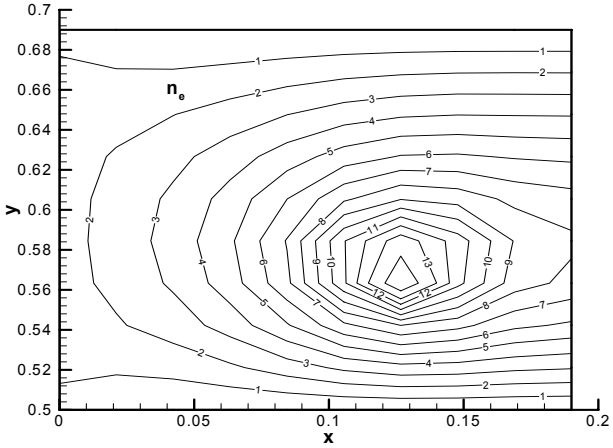

Figure 10. Plasma number density contours in m^{-3}.

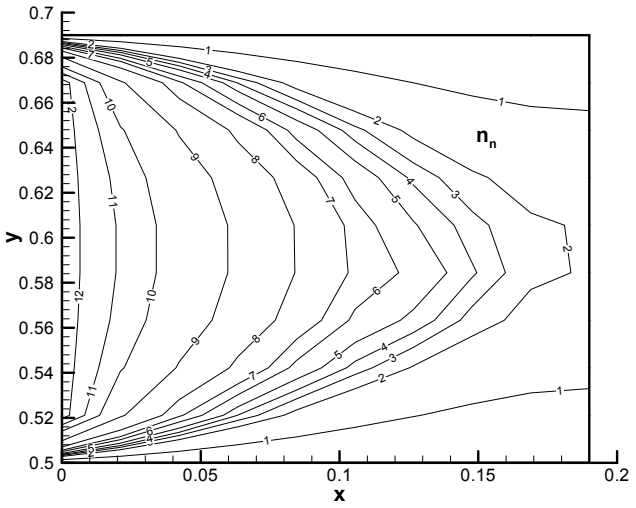

Figure 11. Neutral number density contours in m^{-3}.

CONCLUSIONS

In the present work, the dynamics of a Hall thruster plasma, using the multi-component fluid equation in the presence of secondary electron emission and ion sputter yield has been studied. Owing to the disparate temporal scales of the ions and electrons, ions have been described by the set of time-dependent equations whereas electrons have been described by the steady state equations. Based on the experimental data, a third order polynomial in the electron temperature has been used to describe the ionization processes.

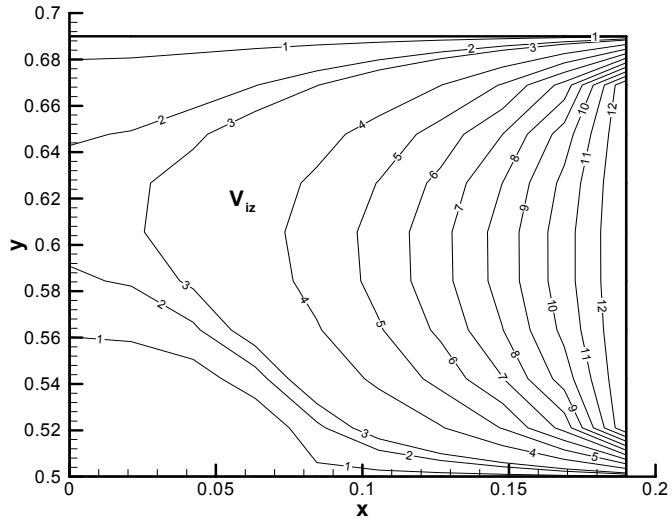

Figure 12. Axial ion velocity contours range between 1 (9 km/s) to 12 (0.2km/s).

The secondary electron emission and ion sputter yield affects the plasma density downstream of the channel. The self-consistent calculation of SEE and Y shows that the plasma-wall loss is less pronounced than when either δ or Y is fixed to a high value. Further, when both SEE and Y are fixed, the plasma number density is lower than the previous case.

The ion velocity profile suggests that due to plasma-wall interaction, most of the "intermediate" energy ions are lost to the wall displaying an "apparent" increase in ion velocity in comparison with the case when SEE is fixed and Y is calculated as a function of electron temperature. The increase in ion velocity is indicative of the loss of the ions to the wall and is reflected in the increased neutral velocity. The electron temperature profiles show expected features and agree with reported experimental data. In the presence of either SEE or Y or both, the electron temperature decreases. Further, downstream of the channel, the temperature is maximum due to the maximum azimuthal energy near the exit. The plasma potential profile compares favorably with the experiment.[19]

Our model has several simplifying assumptions, which will be relaxed in subsequent work. The sputter yield has been calculated assuming $T_i = 0.1\ T_e$. A more consistent approach would require sputter yield to be calculated from the ion energy equation. Further, the quasi-neutrality assumption, which is employed throughout the channel, is not valid near the anode and the sheath effect should be taken into consideration. A proper model of plasma-wall interaction requires the generalization of present 1D model to 2D. We shall generalize the present model in our subsequent work.

The experimental result for 1.6 kW class thruster[21] displays two distinct peak in the ion number density profile located at about 0.02 m and 0.032 m from the anode. These peaks are attributed to different ionization mechanisms – to the electron thermal energy upstream (0.02 m) and to the availability of electron gyration energy at a 0.032 m. These results underline the complexity of the thruster plasma dynamics and inadequacies of the existing numerical models. Several important questions need to be addressed in order to explain the physical mechanism behind the experimentally observed transition from double hump to single hump ion density profile when operating at 1.6 kW and 3 kW.[21] If at 1.6 kW, plasma undergoes a unique ionization-recombination-ionization cycle, then such behavior should be reflected in the neutral velocity and density profiles. We anticipate corresponding to the loss of slow neutrals due to ionization, i.e. number of fast neutrals increase), then decrease and again an increase. Also,

the neutral number density should exhibit an initial decrease, then an increase and again a decrease in its number density. It points to the necessity of generalizing the numerical model on the one hand and further experimental investigation of the thruster plasma dynamics on the other hand.

ACKNOWLEDGEMENTS

This work is supported by NASA GRC research Grant no. NAG3-2520 with David Jacobson as the technical monitor. The authors gratefully acknowledge the technical discussions with Robert Jankovsky, Dave Manzella, Peter Peterson. The first author also recognizes the support of National Academy of Science's NRC fellowship during part of this work.

REFERENCES:

[1]A.I. Morozov and V.V. Savelyev, in Review of Plasma Physics, edited by B.B. Kadomtsev and V.D. Shafranov (Consultant Bureau, New York, 2000), Vol. 21, p. 203.
[2]V.V. Zurin, H.R. Kaufman and R.S. Robinson, Plasma Sources Sci. Technol. 8, 1 (1999).
[3]R. Jankovsky, S. Tverdokhlebov and D. Manzella, 35th Joint Propulsion Conference, 1999 (AIAA, Washington DC, 1999), AIAA-99-2949.
[4]V. Kim, J. Propulsion and Power 14, 736 (1998).
[5]L. Jolivet and J.F. Roussel, 3rd Int. Conf. On Spacecraft propulsion, Cannes, ESA/CNES, (2000).
[6]E. Choueiri, Phys. Plasmas 8, 1411 (2001).
[7]J. P. Boeuf and L. Garigues, J. of Applied Phys. 84, 3541 (1998).
[8]E. Ahedo, P. Martinez and M. Martinez-Sanchez, Phys. Plasmas 8, 3058 (2001).
[9]K. Komurasaki and Y. Arakawa, J. Propulsion and Power 11, 1317 (1995).
[10]E. Ahedo, P. Martinez-Cerezo and M. Martinez-Sanchez, in Proceedings of the 37th Joint Propulsion Conference, Salt Lake City, Utah, 2001, AIAA 2001-3323.
[11]J. M. Fife, Ph.D thesis, MIT, 1998.
[12]A. Fruchtman, N. J. Fisch and Y. Raitses, Phys. Plasmas 8, 1048 (2001).
[13]M. Keidar, I.D. Boyd and I.I.Beilis, Phys. Plasmas 8, 5315 (2001).
[14]S. Roy and B.P. Pandey, in Proceedings of the 27th International Electric Propulsion Conference, Pasadena, California, 2001 (The Electric Rocket Propulsion Society, Worthington, OH, 2001), IEPC-2001-049.
[15]S. Roy and B.P. Pandey, Phys. Plasmas 9, 4052 (2002).
[16]S. Roy and B.P. Pandey, J. Plasma Phys., (in press), 2002.
[17]M. J. Barlow, Mon. Not. R. Astr. Soc., 183, 377 (1978).
[18]Y. Garnier, V. Viel, J.F.Roussel, D.Pagnon, L. Magne and M. Touzeau, IEPC-99-083, Electric propulsion rocket society, 1999.
[19]W.A. Hargus Jr. and M.A. Cappelli, J. Propulsion and Power 18, 159 (2002).
[20]A.M. Bishaev and V. Kim, Soviet Physics, Technical Physics, 23(9) 1055 (1978).
[21]J.M. Haas and A.D. Gallimore, AIAA-00-3422, 36th Joint Propulsion Conf. (JPC) Huntsville, AL, July 16-19, 2000.
[22]D. Balagangadhar and S. Roy, Comp. Methods Appl. Mech. Engr. 190(42) 5465 (2001).
[23]R.D. Richtmyer and K.W. Morton, Difference Methods for Initial-Value Problems, 2d ed. (Interscience Publishers, Wiley, New York, 1967).